

**Bloch point structure in a magnetic nanosphere**Oleksandr V. Pylypovskyi,<sup>1</sup> Denis D. Sheka,<sup>1,2,\*</sup> and Yuri Gaididei<sup>2</sup><sup>1</sup>*Taras Shevchenko National University of Kiev, 01601 Kiev, Ukraine*<sup>2</sup>*Institute for Theoretical Physics, 03143 Kiev, Ukraine*

(Received 20 December 2011; revised manuscript received 1 March 2012; published 1 June 2012)

A Bloch point singularity can form a metastable state in a magnetic nanosphere. We classify possible types of Bloch points and analytically derive the shape of the magnetization distribution for different Bloch points. We show that an external gradient field can stabilize the Bloch point: The shape of the Bloch point becomes radially dependent. We compute the magnetization structure of the nanosphere, which is in good agreement with performed spin-lattice simulations.

DOI: [10.1103/PhysRevB.85.224401](https://doi.org/10.1103/PhysRevB.85.224401)

PACS number(s): 75.10.Hk, 75.40.Mg, 05.45.—a

**I. INTRODUCTION**

Topological singularities are widely recognized as a key for understanding the behavior of a wide variety of condensed-matter systems. Linear topological singularities, such as dislocations, disclinations, and vortices play a crucial role in low-dimensional phase transitions,<sup>1</sup> crystalline ordering on curved surfaces,<sup>2</sup> rotating trapped Bose-Einstein condensates,<sup>3</sup> etc. Recent advances in microstructuring technology have made it possible to fabricate various nanoparticles with well-prescribed geometry. Much recent research in this field has focused on the statics and dynamics of topological singularities in nanoscale confined systems: Essentially, inhomogeneous states can be realized in magnetic nanoparticles<sup>4–6</sup> and ferroelectric nanoparticles.<sup>7</sup> As a result of the competition between exchange and magnetic dipole-dipole interactions, the ground state of magnetic disks with sizes larger than some tens of nanometers is a flux-closure vortex state.

Besides linear singularities, there also exist so-called point singularities, such as monopoles, Bloch points, and boojums. For example, hedgehog (monopole) singularities play a crucial role in the behavior of matter near quantum phase transitions that are seen in a variety of experimentally relevant two-dimensional antiferromagnets,<sup>8</sup> boojums are relevant in superfluid He-3,<sup>9</sup> and Bloch points along with Bloch lines are principal in the understanding of magnetic bubble dynamics.<sup>4,10</sup>

The concept of point singularities in magnetism was introduced by Feldtkeller,<sup>11</sup> who considered different magnetization distributions around the singularity and proposed the first estimations of the Bloch point shape. Later, Döring<sup>12</sup> studied how magnetostatic energy governed the Bloch point structure by selecting the rotation angle inside the Bloch point. Bloch point singularities were directly observed in yttrium iron garnet crystals.<sup>13</sup> During the last decade, Bloch points were also studied by micromagnetic simulations in nanowires,<sup>14</sup> in bubble materials,<sup>15</sup> and in disk-shaped<sup>16,17</sup> and astroid-shaped nanodots.<sup>18</sup> The ultrafast switching of the vortex core magnetization opens doors to consider the vortex state nanoparticles as promising candidates for magnetic elements of storage devices. There are different scenarios of the switching process: (i) The symmetric or so-called punch-through core reversal takes place under the action of a dc magnetic field applied perpendicularly to the magnet plane.<sup>9,16,19,20</sup> This reversal process, as a rule, is mediated by

the creation of two Bloch points.<sup>16</sup> However, the single Bloch point scenario was also mentioned in Thiaville *et al.*<sup>16</sup> (ii) The switching, under the action of different in-plane ac magnetic fields or by spin-polarized currents,<sup>21–26</sup> is accompanied by the temporary creation and annihilation of the vortex-antivortex pair. The latter is accompanied by Bloch point creation.<sup>17</sup>

The purpose of the current paper is to study the magnetization structure of the Bloch point in the spherical nanosized particle. As opposed to bubble films where the static Bloch point results from the transition between Bloch lines<sup>4,10</sup> and vortex nanodots where the Bloch point dynamically appears during the vortex core switching process,<sup>16,21</sup> the nanosphere is a natural geometry where the Bloch point forms a metastable static configuration. Such a singularity is, in some respect, the only stable singularity in the ferromagnet.<sup>16</sup> We consider different types of Bloch points and classify them in terms of vortex parameters. The conventional magnetization distribution in the Bloch point is generalized for the radially dependent one. Such radial distribution becomes important for the Bloch point nanosphere under the action of a nonhomogeneous magnetic field. We show that a radial gradient field can stabilize the Bloch point and we compute the magnetization structure, which is in good agreement with performed spin-lattice simulations.

The paper is organized as follows. In Sec. II, we describe the model and present the classification of different Bloch point types (Sec. II A). The energetic analysis and the Bloch structure is analyzed in Sec. II B. In order to stabilize the Bloch point inside the nanosphere, we consider the influence of an external gradient field on the magnetization structure. The Bloch point solution becomes radially dependent: We calculate the magnetization structure analytically in Sec. III. In Sec. IV, we study the Bloch point structure numerically, in particular, the problem of stability. We discuss our results in Sec. V. In the Appendix, we analyze the Bloch point structure under the influence of weak fields using the linearized equations.

**II. THE MODEL AND THE BLOCH POINT SOLUTIONS**

Let us consider the classical isotropic ferromagnetic sphere of radius  $R$ . The continuum dynamics of the magnetization can be described in terms of the magnetization unit vector  $\mathbf{m} = \mathbf{M}/M_S = (\sin \Theta \cos \Phi, \sin \Theta \sin \Phi, \cos \Theta)$ , where  $\Theta$  and  $\Phi$  are, in general, functions of the coordinates and the

time, and  $M_S$  is the saturation magnetization. The total energy  $E$  of such a sphere, normalized by  $4\pi M_S^2 V$  with  $V = \frac{4}{3}\pi R^3$ , reads

$$\mathcal{E} = \mathcal{E}^{\text{ex}} + \mathcal{E}^{\text{f}} + \mathcal{E}^{\text{ms}}. \quad (1a)$$

The first term in Eq. (1a) is the dimensionless exchange energy,

$$\mathcal{E}^{\text{ex}} = \frac{3}{8\pi} \varepsilon \int d\mathbf{r} [(\nabla\Theta)^2 + \sin^2\Theta (\nabla\Phi)^2], \quad (1b)$$

with  $\varepsilon = \ell^2/R^2$  being the reduced exchange length,  $\ell = \sqrt{A/4\pi M_S^2}$  being the exchange length,  $A$  being the exchange constant, and  $\mathbf{r} = (x, y, z)/R$  being the reduced radius vector. The second term determines the interaction with external magnetic field  $\mathbf{H}$ ,

$$\mathcal{E}^{\text{f}} = -\frac{3}{4\pi} \int d\mathbf{r} (\mathbf{m} \cdot \mathbf{h}), \quad (1c)$$

where  $\mathbf{h} = \mathbf{H}/4\pi M_S$  is a reduced external field. We will discuss the influence of the external field later, see Sec. III. The last term determines the reduced magnetostatic energy,

$$\mathcal{E}^{\text{ms}} = -\frac{3}{8\pi} \int d\mathbf{r} (\mathbf{m} \cdot \mathbf{h}^{\text{ms}}), \quad (1d)$$

where  $\mathbf{h}^{\text{ms}} = \mathbf{H}^{\text{ms}}/4\pi M_S$  is a reduced magnetostatic field  $\mathbf{H}^{\text{ms}}$ . Magnetostatic field  $\mathbf{h}^{\text{ms}}$  satisfies the Maxwell magnetostatic equations,<sup>4,5</sup>

$$\nabla \times \mathbf{h}^{\text{ms}} = 0, \quad \nabla \cdot \mathbf{h}^{\text{ms}} = 4\pi\lambda, \quad (2)$$

which can be solved using a magnetostatic potential  $\mathbf{h}^{\text{ms}} = -\nabla\psi$ . The sources of field  $\mathbf{h}^{\text{ms}}$  are magnetostatic charges: volume charges  $\lambda \equiv -(\nabla \cdot \mathbf{m})/4\pi$  and surface ones  $\sigma \equiv (\mathbf{m} \cdot \mathbf{n})/4\pi$  with  $\mathbf{n}$  being the external normal. The magnetostatic potential inside the sample reads

$$\psi(\mathbf{r}) = \int_V d\mathbf{r}' \frac{\lambda(\mathbf{r}')}{|\mathbf{r} - \mathbf{r}'|} + \int_S dS' \frac{\sigma(\mathbf{r}')}{|\mathbf{r} - \mathbf{r}'|} \quad (3a)$$

$$\equiv \frac{1}{4\pi} \int_V d\mathbf{r}' (\mathbf{m}(\mathbf{r}') \cdot \nabla_{\mathbf{r}'}') \frac{1}{|\mathbf{r} - \mathbf{r}'|}. \quad (3b)$$

The equilibrium magnetization configuration is determined by minimization of the energy functional (II), which leads to

the following set of equations:

$$\varepsilon \nabla^2 \mathbf{m} = \nabla \psi, \quad \nabla^2 \psi = \nabla \cdot \mathbf{m}. \quad (4)$$

### A. Classification of singularities

Let us start the Bloch point as a particular solution of Eq. (4). In the exchange approach, the simplest hedgehog-type Bloch point is characterized by the magnetization distribution of the form  $\mathbf{m} = \mathbf{r}/r$  with a singularity at the origin. Using a spherical frame of reference for the radius vector  $\mathbf{r}$  with the polar angle  $\vartheta$  and the azimuthal one  $\varphi$ , one can describe the magnetization angles of such a Bloch point as follows:  $\Theta = \vartheta$  and  $\Phi = \varphi$ . The energy of the Bloch point in the exchange approach reads<sup>12</sup>

$$\mathcal{E}_0^{\text{ex}} = 3\varepsilon, \quad E_0^{\text{ex}} = 4\pi AR. \quad (5)$$

This interaction is invariant with respect to the joint rotation of all magnetization vectors, which gives the possibility for considering a family of solutions with different rotation angles.<sup>11,12</sup>

We consider the following singular magnetization distribution:

$$\Theta(\vartheta) = p\vartheta + \pi(1-p)/2, \quad \Phi(\varphi) = q\varphi + \gamma, \quad (6)$$

$$p, q = \pm 1,$$

which describes a three-parameter Bloch point. We refer to the parameter  $q = \pm 1$  as the vorticity of the Bloch point and  $p = \pm 1$  as its polarity using the conventional symbols for magnetic vortices. The last parameter  $\gamma$  describes the azimuthal rotational angle of the Bloch point.<sup>11,12</sup>

We refer to the micromagnetic singularity (6) as  $\text{BP}_q^p$ . For example, the hedgehog-type Bloch point is a vortex Bloch point with positive polarity ( $p = 1$ ,  $q = 1$ ,  $\gamma = 0$ ). The schematic of magnetization distribution in different types of Bloch points is presented in Fig. 1. The analogy between Bloch point and vortices comes from the vortex polarity switching process under the action of a dc perpendicular magnetic field.<sup>16</sup> A single Bloch point can be imagined as a composite of two vortices with opposite polarities: Such a singularity can appear in three-dimensional (3D) Euclidean space during the vortex polarity switching process in antiferromagnets.<sup>8,27</sup> Due to the equivalence of two face surfaces of the nanodot, the vortex

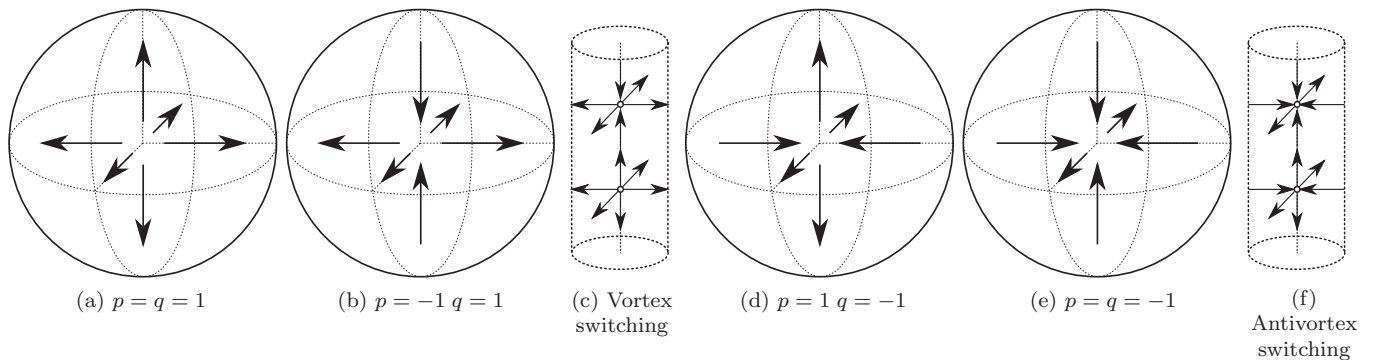


FIG. 1. Schematic of different types of Bloch points. Magnetization distribution in azimuthal vortex Bloch points in a sphere, see (a) and (b), and both Bloch points in the axial part of the cylinder-shaped sample during the vortex polarity switching process, see (c). The same for the azimuthal antivortex Bloch points, see (d) and (e), and both singularities in the axial part of the astroid-shaped sample during the switching, see (f). During the switching process shown in (c) and (f), two Bloch points move along the disk axis in opposite directions and finally annihilate halfway.

polarity switching is mediated, as a rule, by the creation of two Bloch points (symmetric or so-called punch-through mechanism), see Fig. 1(c). They are injected from the ends of the nanodot and annihilate on its axis.<sup>16</sup> All four distributions for different signs of  $p$  and  $q$  can be observed during symmetrical Bloch points' injection in the polarity switching process of vortices<sup>16</sup> [Fig. 1(c)] and antivortices<sup>18</sup> [Fig. 1(f)].

Topological properties of the Bloch point can be described by the topological (Pontryagin) index,

$$Q = \frac{1}{4\pi} \int \sin \Theta(\mathbf{r}) d\Theta(\mathbf{r}) d\Phi(\mathbf{r}) = pq. \quad (7)$$

Different Bloch point distributions with equal  $Q$  are topologically equivalent: e.g.,  $\text{BP}_{-1}^{-1}$  can be obtained from  $\text{BP}_1^1$  by simultaneous rotation of all magnetization vectors by  $\pi$  in the vertical plane, and  $\text{BP}_{-1}^1$  transforms to  $\text{BP}_1^{-1}$  by rotation by  $\pi/2$  in the vertical plane. Note that similar topological notations were introduced by Malozemoff and Slonzewski<sup>10</sup> for magnetic bubbles.<sup>28</sup>

### B. Magnetization structure of Bloch points

The strongest exchange interaction is isotropic, hence, the exchange energy takes the same values for any rotation angle  $\gamma$ . Such degeneracy is removed under the account of magnetostatic interaction. It is worth noting that the problem of stray field influence on the Bloch point energetics has a long story. Feldtkeller, in his pioneer paper,<sup>11</sup> used a so-called pole avoidance principle, see, e.g., Ref. 29: The magnetostatic charge tries to avoid any sort of volume or surface charge. In this way, he calculated the angle  $\gamma$  from the condition of the total volume magnetostatic charge  $\int \lambda(\mathbf{r}) d\mathbf{r} = 0$ , where  $\lambda(\mathbf{r})$  is the charge density. For the Bloch point given by ansatz (6), it has a form  $\lambda(\mathbf{r}) = -[p \sin^2 \vartheta + \cos \gamma (\cos^2 \vartheta + 1)]/4\pi r$  and leads to the rotation angle,

$$\gamma_F = \arccos\left(-\frac{p}{2}\right) = \begin{cases} 120^\circ, & p = +1, \\ 60^\circ, & p = -1. \end{cases} \quad (8)$$

It is interesting to note that the same value  $\gamma_F$  also corresponds to the absence of the total surface charge  $\int \sigma(\mathbf{r}) dS = 0$  where the surface charge density is  $\sigma(\mathbf{r}) = (p \cos^2 \vartheta + \cos \gamma \sin^2 \vartheta)/4\pi$ .

Another approach was put forward by Döring,<sup>12</sup> who determined the equilibrium angle of  $\gamma$  by minimizing the energy,

$$\mathcal{E}_D^{\text{ms}} = \frac{3}{8\pi} \int_V d\mathbf{r} (h^{\text{ms}})^2, \quad (9)$$

and obtained

$$\gamma_D = \arccos\left(-\frac{11}{29}\right) \approx 112.3^\circ. \quad (10)$$

However, one has to emphasize that the equilibrium angle (10) minimizes only the inner part of the magnetostatic energy because the integration in Eq. (9) is carried over the sample volume  $V$ , while the outer part of the stray field is ignored. Note that a similar approach was used in a quite recent paper<sup>30</sup> where a magnetization contraction was taken into account.

The aim of this section is to find the equilibrium rotation angle which minimizes the total magnetostatic energy. In order

to derive the magnetostatic energy of Bloch points (6), we first calculate magnetostatic potential (3b) using an expansion of  $1/|\mathbf{r} - \mathbf{r}'|$  over the spherical harmonics,

$$\frac{1}{|\mathbf{r} - \mathbf{r}'|} = \frac{1}{r_>} \sum_{l=0}^{\infty} \sum_{m=-l}^l \frac{4\pi}{2l+1} \left(\frac{r_<}{r_>}\right)^l Y_{lm}(\vartheta, \varphi) Y_{lm}^*(\vartheta', \varphi'),$$

with  $r_< = \min(r, r')$  and  $r_> = \max(r, r')$ , which results in

$$\psi_{q=1}^p(\mathbf{r}) = p\pi r + \frac{\pi}{3}(9r - 8) \cos \gamma + \pi r(p - \cos \gamma) \cos^2 \vartheta, \quad (11a)$$

$$\psi_{q=-1}^p(\mathbf{r}) = p\pi r(1 + \cos^2 \vartheta) + \pi r \cos(2\varphi + \gamma) \sin^2 \vartheta. \quad (11b)$$

Simple calculations show that the magnetostatic energy of the antivortex Bloch point does not depend on  $\gamma$  and  $\mathcal{E}_{q=-1}^{\text{ms}} = 7/30 \approx 0.23$ . In contrast to this, the vortex Bloch point energy depends on rotation angle  $\gamma$  and has the form

$$\mathcal{E}_{q=1}^{\text{ms}p}(\gamma) = \frac{1}{30}(7 + 4p \cos \gamma + 4 \cos 2\gamma). \quad (12)$$

The equilibrium value of rotation angle  $\gamma_0$  corresponds to the minimum of the energy (12). It gives

$$\gamma_0 = \arccos\left(-\frac{p}{4}\right) \approx \begin{cases} 105^\circ, & p = +1, \\ 76^\circ, & p = -1. \end{cases} \quad (13)$$

Let us compare Bloch point energies (12) for the above-mentioned approaches: The energy of the Feldtkeller<sup>11</sup> Bloch point is  $\mathcal{E}_{q=1}^{\text{ms}p}(\gamma_F) = 0.1$ , for the Döring<sup>12</sup> Bloch point, one has  $\mathcal{E}_{q=1}^{\text{ms}}(\gamma_D) \approx 0.088$ , and the result by Elías and Verga<sup>30</sup> is  $\mathcal{E}_1^{\text{ms}}(\gamma_{EV}) \approx 0.089$ . The minimal energy has a Bloch point with rotation angle  $\gamma_0$ , see Eq. (13),

$$\mathcal{E}_{q=1}^{\text{ms}p}(\gamma_0) = \frac{1}{12} \approx 0.083. \quad (14)$$

In order to verify our results, we performed numerical spin-lattice simulations, see details in Sec. IV. We compare analytical dependence  $\mathcal{E}_{q=1}^{\text{ms}p=1}(\gamma)$ , see Eq. (12), with the discrete energy (24), extracted from simulations, see Fig. 2. Both dependencies are matched in maximum at  $\gamma = 0$ . Comparison can be provided by calculating the energy gain  $\Delta \mathcal{E}(\gamma) = \mathcal{E}_{\text{max}}^{\text{ms}} - \mathcal{E}^{\text{ms}}(\gamma)$  for different rotation angles  $\gamma$ . According to the

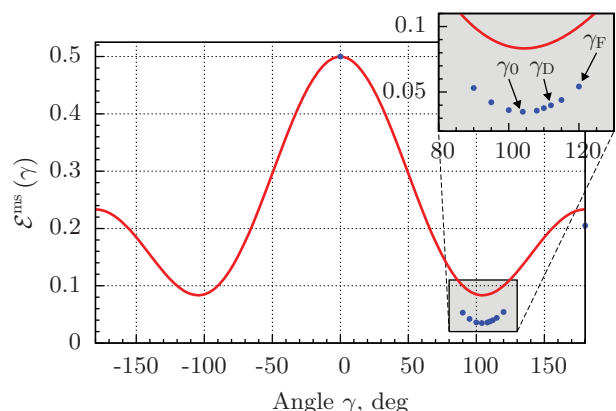


FIG. 2. (Color online) The Bloch point energy vs the rotation angle for  $\text{BP}_1^1$ : analytical result (12) (solid curve) and simulations (symbols). Simulations parameters: sphere diameter  $2R = 35a_0$ , exchange length  $\ell = 3.95a_0$ , and damping parameter  $\eta = 0.5$ .

simulation results, the energy gains for the above-mentioned angles read

$$\Delta \mathcal{E}(\gamma_F) \approx 0.446, \quad \Delta \mathcal{E}(\gamma_D) \approx 0.460, \quad \Delta \mathcal{E}(\gamma_0) \approx 0.465.$$

The maximum energy gain takes place for  $\gamma_0$ , which corresponds to the energy minimum in good agreement with our analytical result (13).

### III. THE BLOCH POINTS IN AN EXTERNAL FIELD

The Bloch point does not form a ground state of a magnetic sphere. It corresponds to the saddle point (sphaleron) of the energy functional.<sup>31</sup> This brings up the question: How to stabilize the Bloch point? In this section, we show that one way to achieve this goal is to apply a magnetic field, which has the same symmetry as the hedgehog Bloch point with  $\mathbf{m} = \mathbf{r}/r$ , i.e., a radially symmetric magnetic gradient magnetic field in the form

$$\mathbf{h} = b\mathbf{r}. \quad (15)$$

Under the action of the space-dependent magnetic field (15), the magnetization distribution also becomes space dependent. We take into account possible dependence by the following radial Bloch point ansatz:

$$\Theta(\vartheta) = p\vartheta + \pi(1-p)/2, \quad \Phi(r, \varphi) = q\varphi + \gamma(r), \quad (16)$$

with a radially dependent parameter  $\gamma(r)$  in comparison with Eq. (6). The form of this ansatz will be justified by numerical simulations in Sec. IV.

Inserting Eq. (16) into Eq. (1b) for the exchange energy of such magnetization distributions, we get

$$\mathcal{E}^{\text{ex}} = 3\varepsilon + \varepsilon \int_0^1 \left( \frac{d\gamma}{dr} \right)^2 r^2 dr. \quad (17a)$$

The magnetostatical potential of the Bloch point (16) reads

$$\begin{aligned} \psi_{q=1}^{p=1}(\mathbf{r}) = & -\frac{4\pi}{3} \int_r^1 [1 + 2 \cos \gamma(r')] dr' \\ & - \frac{4\pi}{3} \frac{3 \cos^2 \vartheta - 1}{r^3} \int_0^r r'^3 [\cos \gamma(r') - 1] dr'. \end{aligned}$$

Here and below, we consider the case of BP<sub>1</sub> only. The magnetostatic energy of such a Bloch point has the form

$$\mathcal{E}^{\text{ms}} = \frac{1}{10} \int_0^1 r^2 [7 + 4 \cos \gamma(r) + 4 \cos 2\gamma(r)] dr. \quad (17b)$$

From Eq. (1c), we obtain that the Bloch point interaction with a magnetic field can be expressed as follows:

$$\mathcal{E}^{\text{f}} = -2b \int_0^1 r^3 \cos \gamma(r) dr. \quad (17c)$$

By minimizing the total energy  $\delta \mathcal{E} / \delta \gamma = 0$ , we obtain that the equilibrium distribution  $\gamma(r)$  is a solution of the following nonlinear differential equation:

$$\varepsilon \frac{d^2 \gamma}{dr^2} + \frac{2\varepsilon}{r} \frac{d\gamma}{dr} + \frac{1}{5} \sin \gamma + \frac{2}{5} \sin 2\gamma - b r \sin \gamma = 0 \quad (18)$$

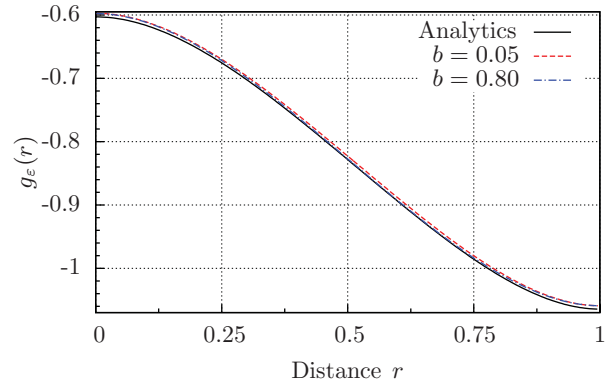


FIG. 3. (Color online) Reduced rotation angle  $g_\varepsilon(r)$ , see Eq. (20) for different field intensities and  $\varepsilon = 0.05$ : analytical result (A1) (solid curve) and numerical solution of Eq. (18) (dashed curves).

augmented by boundary conditions of the form

$$\left. \frac{d\gamma}{dr} \right|_{r=0} = \left. \frac{d\gamma}{dr} \right|_{r=1} = 0. \quad (19)$$

In the case of weak fields, one can linearize Eq. (18) in the vicinity of spatially uniform solution (13) and obtain that

$$\gamma(r) \approx \gamma_0 + b g_\varepsilon(r), \quad |b| \ll 1. \quad (20)$$

An explicit form of the function  $g_\varepsilon(r)$  is calculated in the Appendix. The comparison with the numerical solution of Eq. (18) shows quite good agreement up to relatively strong fields ( $b \lesssim 1$ ), see Fig. 3.

Another limiting case is realized in the case of strong magnetic fields when the Bloch point magnetization is parallel to the external field. In this case, the rotation angle is  $\gamma = 0 \pmod{\pi}$ .

To describe the behavior of the Bloch point in a critical region  $b \approx b_c$  where the spatially nonuniform distribution transforms to the spatially uniform one, we use a variational approach with a two-harmonics trial function  $\gamma(\mathbf{r}) \approx \alpha_0 + \alpha_1 \cos \pi r$ . Near the critical point,  $\alpha_0, \alpha_1 \ll 1$ . We expand the total energy in a Taylor series up to the fourth order with respect to  $\alpha_0$  and to the second order with respect to  $\alpha_1$ . By excluding  $\alpha_1$  and keeping terms not higher than  $\alpha_0^4$ , we get

$$\mathcal{E}(\gamma) \approx \mathcal{E}_0 + p_2(b, \varepsilon) \alpha_0^2 + p_4(b, \varepsilon) \alpha_0^4. \quad (21)$$

The energy (21), as a function of  $\alpha_0$ , has a double-well shape [ $p_2(b, \varepsilon) < 0$ ] for  $b < b_c$  with the critical magnetic field  $b_c$  given by

$$b_c(\varepsilon) \approx 1.8 - 21.6\varepsilon + \sqrt{0.4 - 20.2\varepsilon + 467\varepsilon^2}. \quad (22)$$

In the critical region, when  $0 < b_c(\varepsilon) - b \ll b_c(\varepsilon)$ ,

$$\alpha_0(b) \approx a(\varepsilon) \sqrt{b_c(\varepsilon) - b}. \quad (23)$$

For  $b > b_c$ ,  $p_2 > 0$ , and the function Eq. (21) has a minimum for  $\alpha_0 = 0$ . It corresponds to  $\gamma = 0$ . Numerical integration of Eq. (18) for  $\varepsilon = 0.05$  shows that the phase transition occurs when  $b_c \approx 1.47$ , see Fig. 4. It agrees well with the value  $b_c(0.05) \approx 1.46$  obtained from Eq. (22). The critical behavior predicted by Eq. (23) is also confirmed by our numerical simulations [see Fig. 4(a)].

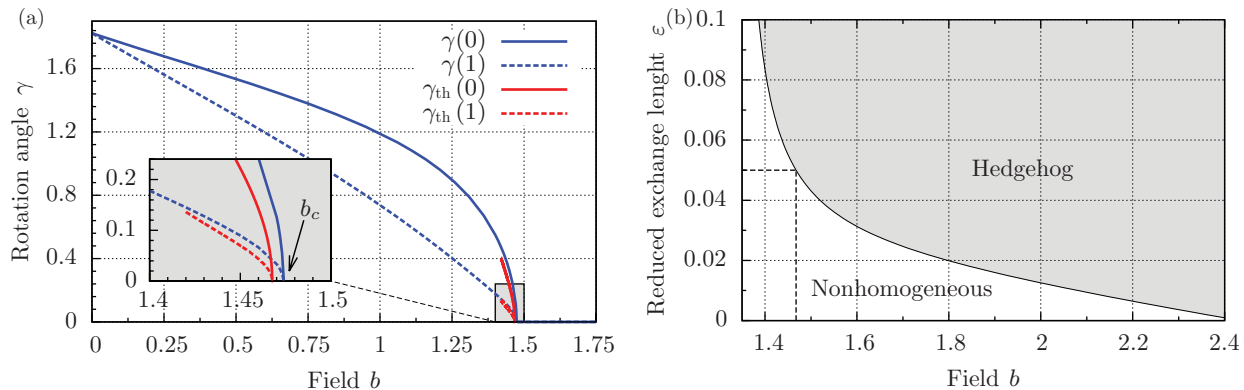


FIG. 4. (Color online) Bloch point under the action of the gradient field. (a) Critical behavior where the rotation angle vs field intensity  $b$  near the critical field  $b_c = 1.47$  from the numerical solution of Eq. (18) (blue curves) and theoretical estimation by Eq. (23) (red curves) with  $\varepsilon = 0.05$ . Solid lines correspond to rotation angle  $\gamma(0)$ , and the dashed line corresponds to  $\gamma(1)$ . (b) Phase diagram for solutions of Eq. (18). The upper (hedgehog) phase corresponds to the solution  $\gamma = 0$ , and the lower (nonhomogeneous) one corresponds to the radially dependent Bloch point with  $\gamma(r)$ . Dashed lines correspond to the analytical result for the critical field  $b_c \approx 1.46$  for  $\varepsilon = 0.05$ , see text.

#### IV. NUMERICAL STUDY OF THE BLOCH POINT STRUCTURE

In order to check analytical results about Bloch point structure, we performed simulations using the in-house developed spin-lattice simulator SLaSi (Ref. 32) that solves the Landau-Lifshitz-Gilbert equation in terms of spins,

$$\frac{d\mathbf{S}_n}{dt} = -\frac{1}{\hbar} \left[ \mathbf{S}_n \times \frac{\partial \mathcal{H}}{\partial \mathbf{S}_n} \right] - \frac{\eta}{S} \left[ \mathbf{S}_n \times \frac{d\mathbf{S}_n}{dt} \right],$$

where  $\mathcal{H}$  is a lattice Hamiltonian of the classical ferromagnet,

$$\mathcal{H} = -\frac{J}{2} \sum_{(n,\delta)} \mathbf{S}_n \cdot \mathbf{S}_{n+\delta} + 2\mu_B \mathbf{H} \sum_n \mathbf{S}_n + 2\mu_B^2 \sum_{n \neq k} \left[ \frac{(\mathbf{S}_n \cdot \mathbf{S}_k)}{r_{nk}^3} - 3 \frac{(\mathbf{S}_n \cdot \mathbf{r}_{nk})(\mathbf{S}_k \cdot \mathbf{r}_{nk})}{r_{nk}^5} \right]. \quad (24)$$

Here,  $\mathbf{S}_n$  is a classical spin vector with fixed length  $S$  in units of action on the site  $n$  of a three-dimensional cubic lattice with lattice constant  $a_0$ ,  $J$  is the exchange integral,  $\mu_B$  is the Bohr magneton,  $\mathbf{r}_{nk}$  is the radius vector between  $n$ th and  $k$ th nodes,  $\eta$  is a damping parameter,  $\mathbf{H}$  is the external magnetic field, and  $\delta$  runs over six nearest neighbors. Integration is performed by the modified fourth- and fifth-order Runge-Kutta-Fehlberg method (RK45) and free spins on the surface of the sample.<sup>33</sup>

Numerically, we checked the Bloch point structure, given by the radially dependent ansatz (16) by modeling a spherically shaped sample with diameter  $2R = 35a_0$  (such a sample consists of 24 464 nodes with nonzero spin) and exchange length  $\ell = 3.95a_0$  ( $\varepsilon = 0.05$ ). In order to stabilize the Bloch point, we applied the gradient magnetic field with  $b = 1.0$ . By modeling the overdamped dynamics, we observed that the Bloch point structure quickly relaxed to the state similar to the one given by Eq. (16): The polar Bloch point angle  $\Theta(\mathbf{r})$  does not deviate from  $\vartheta$  within an accuracy of 0.099 rad. The azimuthal angle is also well described by Eq. (16) with the radially dependent rotation angle  $\gamma(r)$ , see Fig. 5. Simulations were performed for crystallographic directions [111] ( $\vartheta = \pi/4$ ) and [110] ( $\vartheta \approx \pi/2$ , the plane is shifted by  $z = -0.5a_0$  from the origin). From Fig. 5, one can see that

numerical data are well confirmed by analytical curve  $\gamma(r)$ , calculated as a numerical solution of Eq. (18).

To validate our theory, we also performed a direct stability check. Numerically, we checked the stability of the Bloch point against the shift in its position. We start simulations with the Bloch point state using ansatz function (16), which is shifted along the  $\hat{z}$  axis by  $\Delta z = -2a_0$ . We also apply  $\gamma(r, t = 0) = 3^\circ$  in order to break the symmetry. For rapid relaxation, in most of the simulations, we used the overdamped regime (the damping parameter  $\eta = 0.5$ ). We checked the shift in the Bloch point by controlling the total spin projections: Only for the Bloch point, situated at the sample origin, is the total spin  $S_x^{\text{tot}} = S_y^{\text{tot}} = S_z^{\text{tot}} = 0$ .

The temporal evolution of the initially shifted Bloch point is presented in Fig. 6 for the Bloch point sample with  $2R = 35a_0$  (24 456 nodes) in an applied field with  $b = 1$ , see also the Supplemental Material.<sup>34</sup> Originally, the Bloch point was shifted down from the origin, which corresponds to  $S_z^{\text{tot}} > 0$ , see inset (a). During the evolution, a number of magnons are generated, inset (b). After quick damping of the oscillations, the micromagnetic singularity goes to the sample origin, see

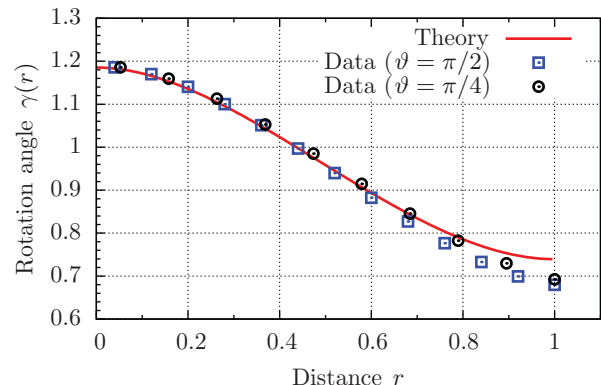


FIG. 5. (Color online) Radial dependence of rotation angle  $\gamma$  in a spherical particle. Line: numerical integration of Eq. (18). Symbols: SLaSi simulations for crystallographic directions [110] and [111]. Parameters are the same as in Fig. 2.

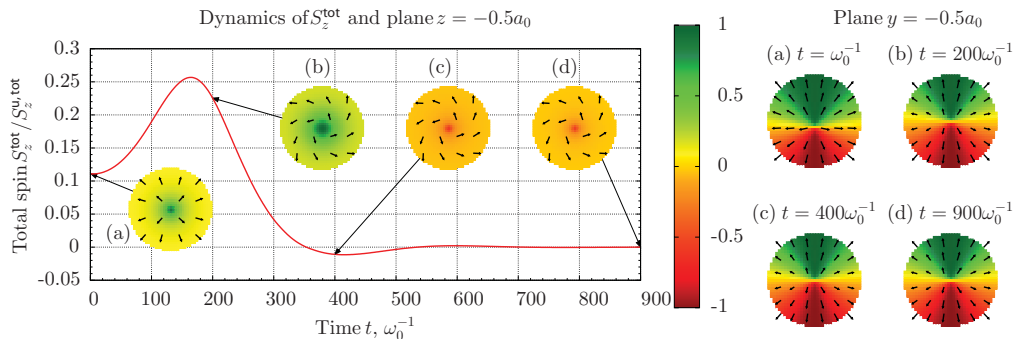


FIG. 6. (Color online) Dynamics of total spin along the  $z$  axis of the sample. The Bloch point is initially shifted by  $\Delta z = -2a_0$  from the center of the sample. The insets show magnetization distribution in  $z = -0.5a_0$  and  $y = -0.5a_0$  planes for different times. The color bar indicates  $S_{z,n}$  for different lattice nodes. The applied field amplitude  $b = 1$  and the other parameters are the same as in Fig. 2.

inset (d). The relaxation process consists of two parts: (i) The rotation angle  $\gamma(r)$  changes its value from the initially uniform one to the final nonhomogeneous state during a time  $\tau_\gamma \approx 500\omega_0^{-1}$ . (ii) The relaxation of the  $S_z^{\text{tot}}$  component of the total spin of the sample took approximately the same time. During all simulation times,  $|S_x^{\text{tot}}| \approx |S_y^{\text{tot}}| \lesssim 10^{-11}$ .

## V. CONCLUSION

To summarize, we studied the magnetization structure of the Bloch point. Despite the fact that the Bloch point, as a simplest 3D topological singularity, was studied for a long time from the pioneering papers by Feldtkeller<sup>11</sup> and Döring,<sup>12</sup> for a review, see also Refs. 4 and 10, the problem of the Bloch point structure still causes discussions.<sup>16,30,35</sup> The point is that the strongest exchange interaction depends only on relative direction of neighboring magnetic moments due to the isotropy of exchange. Therefore, it does not determine the value of rotation angle  $\gamma$ . This rotation angle, which is determined by the magnetostatic interaction, is most questionable: Its value is equal to  $120^\circ$  according to Feldtkeller,<sup>11</sup> to  $112.3^\circ$  following Döring,<sup>12</sup> and to  $113^\circ$  following Elías and Verga.<sup>30</sup> We analyzed the origin of all these results and calculated the equilibrium value, about  $105^\circ$ , see Eq. (12), which minimizes the total magnetostatic energy, not only a part of it.

The next problem appears in the modeling of the Bloch point. It was discussed by Thiaville *et al.*<sup>16</sup> that the modeling of singularity is mesh dependent within the continuum description of micromagnetism. In particular, a mesh-friction effect and a strong mesh dependence of the switching field during the Bloch point mediated vortex switching process was detected using OOMMF micromagnetic simulations.<sup>16</sup> The reason is that micromagnetic simulators consider the numerically discretized Landau-Lifshitz equation, which is valid in continuum theory. Since the Bloch point appears as a singularity of continuum theory, it is always located between mesh points and causes the mesh-dependent effects and, therefore, may be insufficient for describing near-field Bloch point distribution. In contrast to this, spin-lattice simulations are free from these shortages. From the beginning, we considered discrete spins, located on the cubic lattice, and their dynamics was governed by the discrete versions of the Landau-Lifshitz equations. The lattice Hamiltonian allows us to calculate the discrete energy

of the Bloch point similar to the atomiclike calculations by Reinhardt.<sup>36</sup>

Using the in-house developed spin-lattice SLaSi (Ref. 32) simulator, we modeled the Bloch point state nanosphere and checked our analytical predictions about the Bloch point structure. We stabilized the singularity inside the spherical particle by applied gradient magnetic field. The field causes additional radial dependence of rotation angle  $\gamma(r)$  in the Bloch point structure.

## ACKNOWLEDGMENTS

The authors acknowledge computing time on the high-performance computing cluster of the National Taras Shevchenko University of Kyiv<sup>37</sup> and the SKIT-3 Computing Cluster of the Glushkov Institute of Cybernetic of NAS of Ukraine.<sup>38</sup> This work was supported by the Grant of the President of Ukraine Grant No. F35/538-2011. We thank V. Kravchuk for helpful discussions.

## APPENDIX: BLOCH POINT STRUCTURE IN A WEAK FIELD

Here, we consider the magnetization structure of a Bloch point under the action of a weak magnetic field. One has to linearize Eq. (18) on the background of the unperturbed rotation angle  $\gamma_0$ , see Eq. (20), which can be presented as follows:

$$\gamma(r) \approx \gamma_0 + b g_\varepsilon(r), \quad g_\varepsilon(r) = \frac{2\sqrt{5\varepsilon}}{3} f(\lambda r), \quad \lambda = \frac{1}{2} \sqrt{\frac{3}{\varepsilon}}.$$

Here, the function  $f(\xi)$  satisfies the linearized version of Eq. (18),

$$\frac{d^2 f}{d\xi^2} + \frac{2}{\xi} \frac{df}{d\xi} - f = \xi,$$

which can be easily integrated

$$f(\xi) = C_\lambda \frac{\sinh \xi}{\xi} + 2 \frac{\cosh \xi - 1}{\xi} - \xi, \quad (A1)$$

$$C_\lambda = \frac{\lambda^2 - 2\lambda \sinh \lambda + 2 \cosh \lambda - 2}{\lambda \cosh \lambda - \sinh \lambda}.$$

The graphics of the  $g_\varepsilon(r)$  for  $\varepsilon = 0.05$  is presented in Fig. 3 together with the numerical solution of Eq. (18) by the shooting

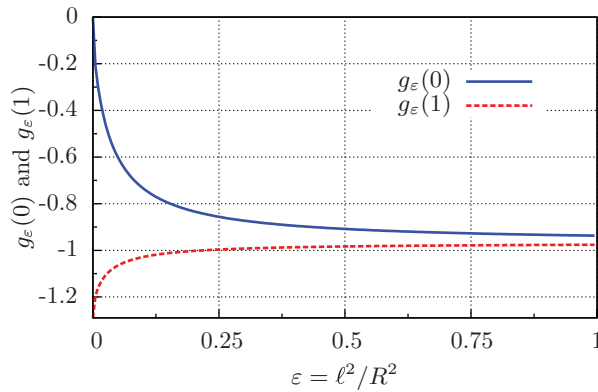


FIG. 7. (Color online) Reduced rotation angle  $g_\varepsilon$  vs reduced exchange length  $\varepsilon$  at  $r = 0$  (solid curve) and  $r = 1$  (dashed curve).

method. Despite the limitation of our analysis by the case of a weak field  $|b| \ll 1$ , the function  $g_\varepsilon(r)$  provides a good approximation for the solution of nonlinear Eq. (18) up to very strong fields  $b \leq 1$  with a relative error of  $|\gamma(r)_{\text{num}} - \gamma(r)_{\text{theor}}|/\gamma(r)_{\text{num}} \leq 0.04$ .

The rotation angle in the Bloch point is essentially influenced by the exchange parameter  $\varepsilon$ , see Fig. 7. In the limiting case of a small particle ( $\varepsilon \gg 1$ ), the role of exchange is dominant, which results in the constant angle  $g_\infty = -\sqrt{15}/4 \approx -0.97$ . In the opposite case  $\varepsilon \ll 1$ , the role of the magnetostatic interaction is enhanced, and this leads to a nonhomogeneous rotational angle distribution. In the limiting case,  $g_0(0) = 0$  and  $g_0(1) = -\sqrt{5}/3 \approx -1.3$ . Such a limiting case is realized in typical soft nanomagnets sized in some tens of nanometers.

\*sheka@univ.net.ua

<sup>1</sup>Phase Transitions and Critical Phenomena, edited by C. Domb and M. S. Green (Academic, New York, 1983), Vol. 7, p. 328; Bond-Orientational Order in Condensed Matter Systems, edited by K. J. Strandburg (Springer, Berlin, 1991), p. 388; F. Yonezawa and T. Ninomiya, in *Topological Disorder in Condensed Matter*, Springer Series in Solid-State Sciences Vol. 46 (Springer, Berlin, 1983), p. 253.

<sup>2</sup>M. J. Bowick and L. Giomi, *Adv. Phys.* **58**, 449 (2009).

<sup>3</sup>A. L. Fetter, *Rev. Mod. Phys.* **81**, 647 (2009).

<sup>4</sup>A. Hubert and R. Schäfer, *Magnetic Domains: The Analysis of Magnetic Microstructures* (Springer-Verlag, Berlin, 1998).

<sup>5</sup>J. Stöhr and H. C. Siegmann, in *Magnetism: From Fundamentals to Nanoscale Dynamics*, Springer Series in Solid-State Sciences Vol. 152 (Springer-Verlag, Berlin/Heidelberg, 2006).

<sup>6</sup>A. P. Guimarães, *Principles of Nanomagnetism*, NanoScience and Technology (Springer-Verlag, Berlin/Heidelberg, 2009).

<sup>7</sup>I. I. Naumov, L. Bellaïche, and H. Fu, *Nature (London)* **432**, 737 (2004).

<sup>8</sup>T. Senthil, A. Vishwanath, L. Balents, S. Sachdev, and M. P. A. Fisher, *Science* **303**, 1490 (2004).

<sup>9</sup>N. D. Mermin, *Phys. Today* **34**(4), 4653 (1981). G. Volovik, *The Universe in a Helium Droplet* (Oxford University Press, Oxford, 2003).

<sup>10</sup>A. P. Malozemoff and J. C. Slonzewski, *Magnetic Domain Walls in Bubble Materials* (Academic, New York, 1979).

<sup>11</sup>E. Feldtkeller, *Z. Angew. Phys.* **19**, 530 (1965).

<sup>12</sup>W. Döring, *J. Appl. Phys.* **39**, 1006 (1968).

<sup>13</sup>Y. P. Kabanov, L. M. Dedukh, and V. I. Nikitenko, *JETP Lett.* **49**, 637 (1989).

<sup>14</sup>R. Hertel and J. Kirschner, *J. Magn. Mater.* **278**, L291 (2004); F. Porrati and M. Huth, *ibid.* **290–291**, 145 (2005); H. Niedoba and M. Labruno, *Eur. Phys. J. B* **47**, 467 (2005); L. Vila, M. Darques, A. Encinas, U. Ebels, J.-M. George, G. Faini, A. Thiaville, and L. Piraux, *Phys. Rev. B* **79**, 172410 (2009).

<sup>15</sup>A. Masseboeuf, T. Jourdan, F. Lançon, P. Bayle-Guillemaud, and A. Marty, *Appl. Phys. Lett.* **95**, 212501 (2009); T. Jourdan,

A. Masseboeuf, F. Lançon, P. Bayle-Guillemaud, and A. Marty, *J. Appl. Phys.* **106**, 073913 (2009).

<sup>16</sup>A. Thiaville, J. M. Garcia, R. Dittich, J. Militat, and T. Schrefl, *Phys. Rev. B* **67**, 094410 (2003).

<sup>17</sup>R. Hertel and C. M. Schneider, *Phys. Rev. Lett.* **97**, 177202 (2006).

<sup>18</sup>X. J. Xing, Y. P. Yu, S. X. Wu, L. M. Xu, and S. W. Li, *Appl. Phys. Lett.* **93**, 202507 (2008).

<sup>19</sup>T. Okuno, K. Shigeto, T. Ono, K. Mibu, and T. Shinjo, *J. Magn. Mater.* **240**, 1 (2002).

<sup>20</sup>V. Kravchuk and D. Sheka, *Phys. Solid State* **49**, 1923 (2007).

<sup>21</sup>B. Van Waeyenberge, A. Puzic, H. Stoll, K. W. Chou, T. Tylliszczak, R. Hertel, M. Fähnle, H. Bruckl, K. Rott, G. Reiss, I. Neudecker, D. Weiss, C. H. Back, and G. Schütz, *Nature (London)* **444**, 461 (2006).

<sup>22</sup>Q. F. Xiao, J. Rudge, B. C. Choi, Y. K. Hong, and G. Donohoe, *Appl. Phys. Lett.* **89**, 262507 (2006).

<sup>23</sup>R. Hertel, S. Gliga, M. Fähnle, and C. M. Schneider, *Phys. Rev. Lett.* **98**, 117201 (2007).

<sup>24</sup>K. Yamada, S. Kasai, Y. Nakatani, K. Kobayashi, H. Kohno, A. Thiaville, and T. Ono, *Nature Mater.* **6**, 270 (2007).

<sup>25</sup>V. P. Kravchuk, D. D. Sheka, Y. Gaididei, and F. G. Mertens, *J. Appl. Phys.* **102**, 043908 (2007).

<sup>26</sup>D. D. Sheka, Y. Gaididei, and F. G. Mertens, *Appl. Phys. Lett.* **91**, 082509 (2007).

<sup>27</sup>E. G. Galkina and B. A. Ivanov, *JETP Lett.* **61**, 511 (1995).

<sup>28</sup>Bloch points in magnetic bubbles were classified by Malozemoff and Slonzewski<sup>10</sup> using the flux  $N$  of the gyrotropic vector. Simple calculations show that the value of such a flux is opposite the topological density (7),  $N = -Q$ .

<sup>29</sup>A. Aharoni, *Introduction to the Theory of Ferromagnetism* (Oxford University Press, Oxford, 1996).

<sup>30</sup>R. Elías and A. Verga, *Eur. Phys. J. B* **82**, 159 (2011).

<sup>31</sup>N. Manton and P. Sutcliffe, in *Topological Solitons*, Cambridge Monographs on Mathematical Physics (Cambridge University Press, Cambridge, UK, 2004).

<sup>32</sup>SLaSi spin-lattice simulations package code available at [<http://slasi.rpd.univ.kiev.ua>].

<sup>33</sup>We take the integration time step  $\Delta t = 0.025\omega_0^{-1}$  for the accuracy  $\Delta S_{\max} = \max_{i,n} |S_{i,n}^4 - S_{i,n}^5| < 0.01$ , where  $\omega_0 = JS^2/\hbar$ ,  $i = x, y, z$  and the superscript for  $S_{i,n}$  indicates the integration order. We used a modified RKF45 scheme where the time step was changed only if the accuracy goal for  $\Delta S_{\max}$  was not reached for avoiding noise from step changing.

<sup>34</sup>Supplemental Material at [<http://slasi.rpd.univ.kiev.ua/sm/pylypovskyi12/>] for a video.

<sup>35</sup>G. Khodenkov, *Tech. Phys.* **55**, 738 (2010).

<sup>36</sup>J. Reinhardt, *Int. J. Magn.* **5**, 263 (1973).

<sup>37</sup>[<http://cluster.univ.kiev.ua/>].

<sup>38</sup>[<http://icybcluster.org.ua/>].